

# Removal of Particulate Contamination from Solid Surfaces Using Polymeric Micropillars

Hadi Izadi,<sup>†</sup> Navneet Dogra,<sup>†</sup> François Perreault,<sup>†</sup> Cynthia Schwarz,<sup>‡</sup> Stefan Simon,<sup>§</sup> and T. Kyle Vanderlick<sup>\*,†</sup>

<sup>†</sup>Department of Chemical and Environmental Engineering, Yale University, 10 Hillhouse Avenue, New Haven, Connecticut 06520, United States

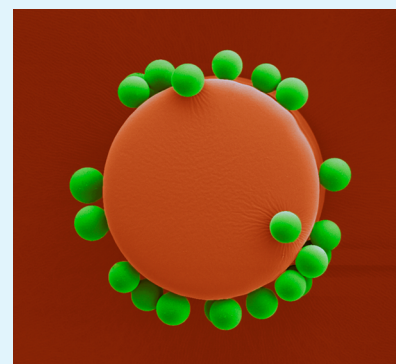
<sup>‡</sup>Yale University Art Gallery, Yale University, 1111 Chapel Street, New Haven, Connecticut 06510, United States

<sup>§</sup>Institute for the Preservation of Cultural Heritage, Yale University, 300 Heffernan Drive, West Haven, Connecticut 06516, United States

## S Supporting Information

**ABSTRACT:** This Research Article describes a novel method for removal of particulate contamination, loosely referred to as dust, from solid surfaces using polymeric micropillars. In this Research Article, we illustrate for the first time that polymeric microfibrils of controlled interfacial and geometrical properties can effectively remove micrometric and submicrometric contaminant particles from a solid surface without damaging the underlying substrate. Once these microfibrils are brought into contact with a contaminated surface, because of their soft and flexible structure, they develop intimate contact with both the surface contaminants and the substrate. While these intrinsically nonsticky micropillars have minimal interfacial interactions with the substrate, we show that they produce strong interfacial interactions with the contaminant particles, granting the detachment of the particles from the surface upon retraction of the cleaning material. The origin and strength of the interfacial interactions at the interfaces between a contaminant particle and both the substrate and the cleaning materials are thoroughly discussed. Unlike flat substrates of the same material, using microfibrillar structures of controlled interfacial and geometrical properties also allows the elimination of the adsorbed particles from the contact interface. Here we demonstrate that by moving the adsorbed particles from the tip to the side of the fibrils and consequently removing them from the contact interface, polymeric microfibrils can clean all contaminant particles from the surface. The effects of the geometrical and interfacial properties of polymeric micropillars on removing the adsorbed particles from the tips of the pillars are fully discussed. This research is not only important in terms of introducing a novel method which can offer a new paradigm for thorough yet nondestructive cleaning of dust particles from solid surfaces, but also it is of fundamental significance for researchers with interests in exploiting the benefits offered by microstructured surfaces in development of interfacially active materials and devices.

**KEYWORDS:** surface cleaning, particulate contamination, micropillars, adhesion, contact electrification



## INTRODUCTION

Removal of micrometric and submicrometric contaminant particles, loosely referred to as dust, from solid surfaces is a critical and exacting challenge in various areas of science and technology, including microelectronics, aerospace, optics, xerography, and adhesive bonding.<sup>1–5</sup> While removal of relatively large ( $>10\ \mu\text{m}$ ) particles from the surface can be simply achieved by blowing them off with a gas jet,<sup>3</sup> removal of smaller, micrometric and submicrometric, particles is usually carried out with wet cleaning techniques, including conventional solvent cleaning methods and more advanced acoustic cleaning approaches.<sup>3,6</sup> Although they are common, traditional wet cleaning techniques present increasing disadvantages, including limited efficiency in removal of submicrometric ( $<0.3\ \mu\text{m}$ ) particles, incompatibility with chemical-sensitive materials, redeposition from contaminated chemicals, environ-

mental damage, and also possible liquid residue causing adhesion of remaining particles.<sup>2,3</sup> For these reasons, removal of dust particles using dry cleaning techniques (e.g., cleaning with laser beam, microabrasive particles, argon/nitrogen aerosols, and carbon dioxide snow jet) has gained increasing attention in recent decades.<sup>3,4,7,8</sup> Although dry cleaning approaches do not have many of the drawbacks of the wet cleaning methods, they have one major disadvantage: they can damage the surface of the substrate upon removal of the surface contaminants.<sup>7,9</sup> In particular, effective dry cleaning approaches mostly rely on usage of energy transfer from an impacting source (e.g., laser beam or accelerated microparticles) to the

**Received:** September 28, 2015

**Accepted:** April 21, 2016

**Published:** April 21, 2016

contaminant particles to provide a sufficient amount of energy to overcome the dust particles adhesion to the surface of the substrate.<sup>3,4</sup> However, mechanical and thermal stresses that these energy sources advantageously use to detach the dust particles from the surface may also adversely cause damage and even material loss at the surface of the substrate itself.<sup>7,9</sup>

In the search for an effective but nondestructive dry cleaning technique for the removal of micrometric and submicrometric particulate contamination from solid surfaces, we report a novel method using microscale fibrillar structures made from an elastic and low-surface-energy polymer. When these polymeric microfibrils are brought into contact with a contaminated surface, because of their soft and flexible nature, they develop intimate contact with both the surface contaminants and the substrate. While these intrinsically nonsticky micropillars have minimal interfacial interactions with the substrate, development of strong interfacial forces between the cleaning material and the contaminant particles facilitates the detachment of the particles from the surface of the substrate upon retraction of the cleaning material. Unlike flat substrates of the same material, using microfibrillar structures of controlled geometrical and interfacial properties also allows the elimination of the adsorbed particles from the contact interface (by moving them from the tip to the side of the fibrils), granting a nondestructive cleaning performance by the fibrillar cleaning material. Here, we will demonstrate for the first time that polymeric microfibrillar structures can offer a new paradigm for thorough cleaning of micrometric and submicrometric dust particles from solid surfaces while leaving the underlying substrate intact.

## RESULTS AND DISCUSSION

In this study, we employed fibrillar structures of various geometrical properties (2–50  $\mu\text{m}$  in diameter with aspect-ratios of  $\sim 2$ ) to remove spherical, monodisperse silica particles (with nominal diameters of 0.26–7.75  $\mu\text{m}$ ), used as the contaminants, from the surface of poly(methyl methacrylate) (PMMA) thin films ( $260 \pm 5$  nm ( $n = 6$ ) in thickness), used as the substrate. An elastic and low-surface-energy polymer, polydimethylsiloxane (PDMS), was used for the fabrication of the fibrillar cleaning materials. PDMS was chosen for this purpose because it has low surface energy and high elasticity, properties that minimize the interfacial interactions and mechanical stresses between the cleaning material and the substrate. On the other hand, as an elastic and electrically nonconductive polymer which can develop intimate contact with other surfaces, PDMS can generate strong interfacial interactions with the contaminant particles, stronger than those between the particles and the substrate (PMMA). Having stronger interfacial interactions at the PDMS/silica interface grants the detachment of the contaminant particles from the PMMA surface upon retraction of the cleaning material from the substrate.

As an initial step in understanding the interfacial interactions of silica particles with the substrate and the cleaning material, the adhesion forces between 7.75  $\mu\text{m}$  silica particles and both PMMA and PDMS were measured using an atomic force microscope. As shown in Figure 1A1 and A2, under the typical preload of 100 nN, the adhesion force ( $F_{\text{pull-off}}$ ) between a 7.75  $\mu\text{m}$  silica particle (Figure 1A3) and PDMS was  $270.6 \pm 10.3$  nN ( $n = 10$ ), about five times larger than that between the particle and PMMA ( $F_{\text{pull-off,PMMA}} = 56.0 \pm 4.2$  nN ( $n = 10$ )). One must question how PDMS can generate larger adhesion forces than PMMA, taking into consideration the range of

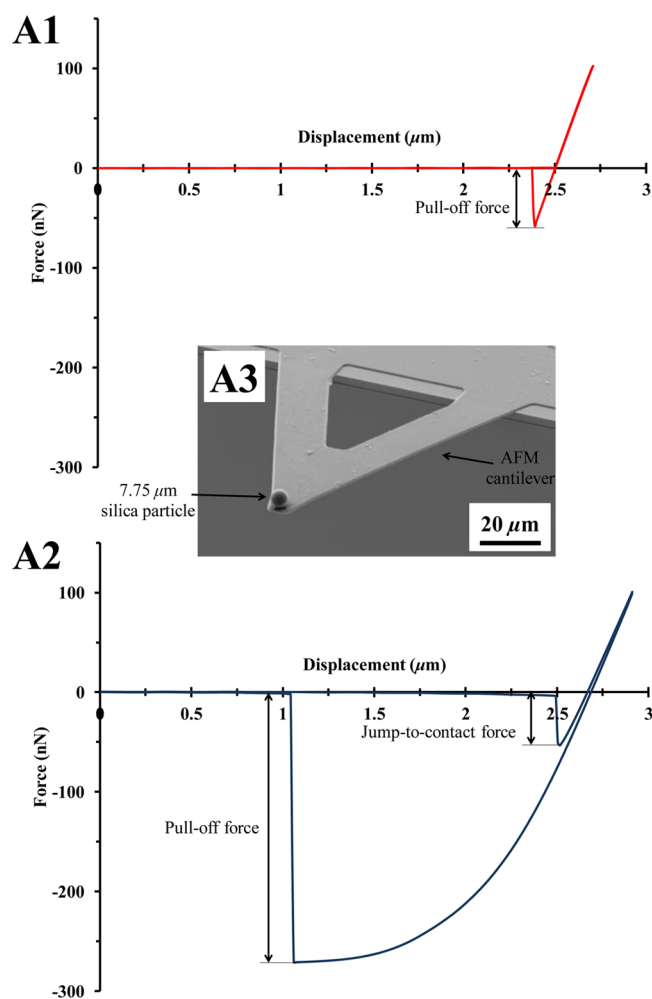


**Figure 1.** Typical indentation traces (force vs displacement) for (A1) a PMMA thin film and (A2) a PDMS flat sheet measured in contact with (A3) a 7.75  $\mu\text{m}$  silica particle which was adhered to a tipless atomic force microscope cantilever.

possible interfacial interactions that hold silica particles to these surfaces. To answer this question, first it should be noted that the possible interfacial interactions at both PDMS/silica and PMMA/silica interfaces can be only van der Waals (vdW), capillary, and/or electrostatic forces; vdW interactions naturally exist between two materials in contact,<sup>10</sup> while capillary interactions become effectual in humid conditions.<sup>10,11</sup> Electrostatic interactions, on the other hand, can be formed upon contact of any two surfaces, even if the contacted surfaces were electrically neutral in the first place.<sup>12,13</sup>

The magnitude of the vdW interaction force between two substrates can be determined by using the Hamaker method.<sup>10</sup> Using this method, the vdW-driven adhesion force ( $F_{\text{vdW}}$ ) interacting between phase 1 (silica microparticles) and phase 2 (PDMS or PMMA) across medium 3 (air) at the separation distance  $D$  can be calculated by  $F_{\text{vdW}} = -A_{132}R/6D^2$ , where  $R$  is the radius of the silica microparticles and  $A_{132}$  is the Hamaker constant between phase 1 and phase 2, interacting across medium 3.<sup>10</sup> The corresponding Hamaker constant for each contact interface (i.e., PDMS/silica and PMMA/silica interface) can be determined according to the Lifshitz model (eq 1). Based on this model

$$A_{132} \approx \frac{3}{4} kT \left( \frac{\epsilon_1 - \epsilon_3}{\epsilon_1 + \epsilon_3} \right) \left( \frac{\epsilon_2 - \epsilon_3}{\epsilon_2 + \epsilon_3} \right) + \frac{3h\nu_e}{8\sqrt{2}} \frac{(n_1^2 - n_3^2)(n_2^2 - n_3^2)}{(n_1^2 + n_3^2)^{1/2}(n_2^2 + n_3^2)^{1/2} \{ (n_1^2 + n_3^2)^{1/2} + (n_2^2 + n_3^2)^{1/2} \}} \quad (1)$$

where  $k$  is Boltzmann's constant,  $T$  is the temperature,  $h$  is Planck's constant, and  $\nu_e$  is the electron absorption frequency (typically around  $3 \times 10^{15}$  1/s).<sup>10</sup>  $\epsilon_1$ ,  $\epsilon_2$ , and  $\epsilon_3$  are the corresponding dielectric constants of phase 1, phase 2, and medium 3, respectively, while  $n_1$ ,  $n_2$ , and  $n_3$  are the refractive indices of phase 1, phase 2, and medium 3, respectively.<sup>10</sup> Using the Lifshitz model and considering the dielectric constants of PDMS, PMMA, and silica as 2.7,<sup>14</sup> 4.0,<sup>15</sup> and 3.8,<sup>10</sup> respectively, and their refractive indices as 1.41,<sup>14</sup> 1.49,<sup>15</sup> and 1.45,<sup>10</sup> the Hamaker constant for the PMMA/silica contact in dry conditions would be equal to  $6.4 \times 10^{-20}$  J, while that for the PDMS/silica contact would be  $5.5 \times 10^{-20}$  J. Knowing the Hamaker constants of the PDMS/silica and PMMA/silica interfaces and assuming that PDMS and PMMA surfaces (with the roughness average ( $R_a$ ) values of  $1.5 \pm 0.1$  ( $n = 5$ ) and  $0.8 \pm 0.1$  nm ( $n = 5$ ), respectively) come into intimate molecular contact with silica particles (i.e.,  $D \approx 0.3$  nm),<sup>10</sup> then according to the Hamaker method, it is expected that PDMS develops similar vdW forces to PMMA ( $F_{\text{vdW,PDMS}} = -0.9 \mu\text{N}$  while  $F_{\text{vdW,PMMA}} = -1.0 \mu\text{N}$ ).

Other than the Hamaker model, the well-known Johnson–Kendall–Roberts (JKR) model can also be employed to determine the magnitude of the vdW interaction force between two substrates in intimate contact.<sup>16</sup> According to this model, the absolute value of the vdW adhesive force between a  $7.75 \mu\text{m}$  silica particle and PMMA is about  $-1.1 \mu\text{N}$ , similar to that between the particle and PDMS ( $F_{\text{vdW,PDMS}} = -1.0 \mu\text{N}$ ) (see the Supporting Information for further details).

It is clear that theoretically, PDMS and PMMA are expected to develop relatively similar vdW forces of about  $1.0 \mu\text{N}$  upon intimate contact with a  $7.75 \mu\text{m}$  silica particle. Even so, the measured adhesion forces ( $F_{\text{pull-off}}$ ) of PDMS were about five times larger than those of PMMA (see Figure 1A1 and A2). More importantly, the actual measured adhesion forces ( $F_{\text{pull-off}}$ ) of these polymers ( $270.6 \pm 10.3$  nN for PDMS and  $56.0 \pm 4.2$  nN for PMMA ( $n = 10$ )) were significantly smaller than the theoretical  $F_{\text{vdW}}$  value of  $\sim 1.0 \mu\text{N}$ , which was expected to be developed if vdW interactions were fully functional at the surface of these polymers.

One of the reasons for the adhesion difference between PDMS and PMMA and also for the deviation of the experimental results from the theoretical estimates is the inability of the chosen polymers to develop an intimate molecular contact with silica particles.<sup>17,18</sup> More specifically, both PDMS and PMMA are required to reach an intimate molecular contact of  $\sim 0.3$  nm with silica particles in order to achieve the estimated vdW adhesion forces of about  $1 \mu\text{N}$ . However, because of natural roughness at the surface of these polymers ( $R_{a,\text{PDMS}} = 1.5 \pm 0.1$  nm ( $n = 5$ );  $R_{a,\text{PMMA}} = 0.8 \pm 0.1$  nm ( $n = 5$ )), achieving this close proximity throughout the entire contact zone, and thus effective vdW interactions at the contact interface, is challenging. To elucidate the importance of the effect of the nanoasperities of the surface of these polymers on declining the magnitude of their vdW interfacial forces, the modified Rumpf model (eq 2) has been employed.<sup>18</sup> According to this model, the vdW interaction force between a smooth spherical particle of radius  $R$  (phase 1) and a flat polymeric

substrate (phase 2, with root-mean-square roughness parameter  $R_{\text{RMS}}$ ) can be calculated using

$$F_{\text{vdW}} = \frac{A_{132}R}{6H_0^2} \left[ \frac{1}{1 + \frac{R}{1.48R_{\text{RMS}}}} + \frac{1}{\left(1 + \frac{1.48R_{\text{RMS}}}{H_0}\right)^2} \right] \quad (2)$$

where  $H_0$  is the distance of closest approach between the two surfaces ( $\sim 0.3$  nm).<sup>18</sup> Using eq 2 and considering that  $R_{\text{RMS,PDMS}} = 1.9 \pm 0.2$  nm ( $n = 5$ ) and  $R_{\text{RMS,PMMA}} = 1.0 \pm 0.1$  nm ( $n = 5$ ), while assuming that the nanoasperities at the surface of these polymers are not deformable, it is expected that PDMS develops vdW forces of about  $4.1$  nN upon contact with a  $7.75 \mu\text{m}$  silica particle, while PMMA should generate vdW forces of about  $13.6$  nN at the same contact. From the estimation of vdW interfacial forces by the modified Rumpf model, it is clear that the presence of nanoasperities at the surface of PDMS and PMMA can result in significant decrease in vdW interfacial forces of these polymers. It should be also noted that in the above analysis, for the sake of simplicity, it has been assumed that the surface of the employed silica particles were atomically smooth. Even so, it is expected that the roughness at the surface of silica particles also partly contribute in decreasing the achievable vdW adhesive forces by increasing the actual separation distance between the particles and the polymer surfaces.

While roughness—even at nanometric and subnanometric scales—can significantly decrease the ultimate vdW interaction force between two substrates, it is expected that most nanoasperities at the surface of soft materials (like PDMS and PMMA) are squeezed out upon contact with a comparatively more rigid material like silica (with Young's modulus of  $\sim 71.7$  GPa).<sup>19</sup> Therefore, to shed light on the effect of the mechanical properties of these polymers and, accordingly, the deformation of their surface nanostructures upon contact with silica particles, the penetration depth ( $\delta$ ) of silica particles into these polymers were calculated using the JKR model (see the Supporting Information for further details). In general, it is expected that all surface asperities with a height equal or smaller than  $\delta$  values are squeezed out during contact with silica particles.<sup>20</sup> According to the JKR model, the penetration depth of a  $7.75 \mu\text{m}$  silica particle in PMMA and PDMS (under the applied load of  $100$  nN) is  $\sim 4$  and  $240$  nm, respectively. Therefore, by considering that the maximum peak height ( $R_p$ ) for PDMS ( $30.4 \pm 7.9$  nm ( $n = 5$ )) is just one-eighth of the particle penetration depth in this polymer, while the penetration depth of the silica particle in PMMA ( $\sim 4$  nm) is smaller than the  $R_p$  value for this polymer ( $5.9 \pm 0.5$  nm ( $n = 5$ )), it is clear that, in comparison to PMMA, PDMS should have generated much better intimate contact with silica particles.

On the whole, it can be inferred that vdW-driven adhesion forces of PDMS, upon contact with a  $7.75 \mu\text{m}$  silica particle, changes in the range of  $4.1$  nN to  $1.0 \mu\text{N}$ , while those of PMMA are between  $13.6$  nN and  $1.1 \mu\text{N}$ . Analysis of vdW interactions also clearly shows that while PDMS and PMMA theoretically have similar ability in formation of vdW interactions upon contact with silica particles, it is expected that PDMS generates larger vdW forces than PMMA, seeing that it develops better intimate contact in comparison to PMMA.

In contrast to vdW forces, the contribution of capillary forces in the overall interfacial interaction forces ( $F_{\text{pull-off}}$ ) of both PDMS and PMMA can be simply neglected. The formation of capillary forces in the current system is very doubtful since all experiments in this study were carried out at a relative humidity (RH) of  $10 \pm 1\%$  ( $T = 20 \pm 1^\circ\text{C}$ ), where adsorption of sufficient amounts of water at the contact interface to form capillary bridges is unlikely.<sup>11,21</sup> Even so, it should be considered that water monolayers still can be adsorbed on the surface of the employed materials (even at this level of humidity), especially the hydrophilic ones.<sup>11,21</sup> Water monolayers do not produce capillary forces, but they can affect—and particularly decrease—the short-range vdW forces between two contacted surfaces.<sup>21</sup> From this perspective and to ascertain whether or not water monolayer adsorption is the cause of the significantly smaller adhesion of PMMA in comparison to PDMS, we considered an extreme case where the hydrophobic PDMS/silica interface was presumed to be completely dry (i.e., vdW forces were considered to be in full effect) while a water monolayer was assumed to be present at the hydrophilic PMMA/silica interface (i.e., vdW forces were declined by a monolayer of water). Considering that a monolayer of water is present at the contact interface between PMMA and silica, the vdW interaction forces still can be calculated by  $F_{\text{vdW}} = -A_{132}R/6D^2$ , but by replacing  $A_{132}$  with  $A_{\text{eff}}$ , the effective Hamaker constant of the system.  $A_{\text{eff}}$  for PMMA/silica can be determined from  $A_{\text{eff}} = fA_{\text{dry}} + \rho f' A_{\text{wet}}$ <sup>21</sup> where  $f$  is the areal fraction of the silica surface which is in direct contact with the PMMA substrate, while  $f'$  is the areal fraction of the silica surface which is in contact with PMMA through a monolayer of water.  $A_{\text{wet}}$  and  $A_{\text{dry}}$  are the Hamaker constants in wet and dry conditions, respectively.  $\rho$  is the relative water coverage of the surface, which can be calculated by the Langmuir adsorption isotherm as

$$\rho = \frac{H}{H + \exp\left(\frac{-E}{kT}\right)} \approx H \exp\left(\frac{E}{kT}\right) \approx 1.22H \quad (3)$$

where  $H$  is the humidity and  $E$  is the adsorption energy, which is typically much smaller than the thermal energy ( $kT$ ) at room temperature.<sup>21</sup> In eq 3, we assumed that for a hydrophilic substrate like PMMA or silica,  $E = (A_w A_s)^{1/2}/16\pi \approx 0.2kT$ ,<sup>21</sup> where  $A_w = 3.7 \times 10^{-20}$  J for water,<sup>10</sup> whereas, according to the Lifshitz model (eq 1),  $A_s$  is equal to  $6.0 \times 10^{-20}$  J for silica and  $6.9 \times 10^{-20}$  J for PMMA. Doing so, the relative water coverage of the surface ( $\rho$ ) for PMMA and silica would be  $\sim 0.12$ . In other words, according to the Langmuir adsorption isotherm, about 12% of the surface of a hydrophilic material (such as PMMA ( $\theta_{\text{PMMA}} = 82 \pm 1^\circ$  ( $n = 8$ )) or silica ( $\theta_{\text{silica}} = 70 \pm 2^\circ$  ( $n = 8$ ))) can get covered with a monolayer of water at RH of  $10 \pm 1\%$ . Using  $f' = 1.2f$  for an intimate contact,<sup>21</sup> and knowing that  $A_{\text{dry}} = 6.4 \times 10^{-20}$  J and  $A_{\text{wet}} = 0.8 \times 10^{-20}$  J for PMMA/silica—according to the Lifshitz model (eq 1), the effective Hamaker constant in the presence of a monolayer of water for PMMA/silica would be equal to  $2.9 \times 10^{-20}$  J, approximately half of the Hamaker constant of PDMS/silica in dry conditions ( $5.5 \times 10^{-20}$  J). Even in this extreme scenario, the Hamaker constant of the dry PDMS/silica interface is only about twice larger than the Hamaker constant of the wet PMMA/silica interface, a significantly lower ratio than the actual 5-fold adhesion difference between PDMS and PMMA (see Figure 1A1 and A2). Therefore, it can be concluded that water monolayer adsorption is certainly not the main reason behind

the significantly smaller adhesion of PMMA in comparison to PDMS, although it may be a minor contributor.

Another cause for the large adhesion difference between PDMS and PMMA upon contact with silica particles can be the difference in electrostatic interactions of these polymers formed via surface charging. In general, when any two—similar or dissimilar—materials touch each other, electric charges transfer from one surface to the other,<sup>12,22</sup> resulting in the development of a net negative charge on one substrate and a net positive charge on the other.<sup>23</sup> Formation of an electrical double layer at the contact interface via this contact electrification (CE) phenomenon, which is usually more pronounced in the case of insulating materials,<sup>24–26</sup> gives rise to electrostatic interactions between the triboelectrically charged objects.<sup>12,13</sup> In order to determine the occurrence of CE and the extent of the electrostatic interactions arising from that in our system, the magnitude of electric charges that build up upon contact of silica with both PDMS and PMMA were measured. Because the direct measurement of CE-generated charge densities during adhesion tests with silica microparticles is technically very difficult, due to very small area of contact, contact charge measurements in this study were carried out upon contact with a  $\sim 25.4$  mm in diameter—polished silica disc ( $R_{\text{a,silica}} = 1.0 \pm 0.1$  nm ( $n = 5$ )).

Using image charge analysis (details can be found in the Experimental section),<sup>12,13,27</sup> the absolute value of the surface charge densities formed upon contact of PDMS with silica were found to be  $1.5 \pm 0.1$  mC/m<sup>2</sup> ( $n = 10$ ), three times larger than those of PMMA with silica ( $0.5 \pm 0.1$  mC/m<sup>2</sup> ( $n = 10$ )). To obtain an approximation of the electrostatic force ( $F_{\text{elc}}$ ) that these surface charge densities can produce, the well-known simple capacitor model (eq 4), which describes the electrostatic interaction force between two charged flat parallel sheets, was employed.<sup>25</sup> According to this model, the magnitude of the electrostatic force ( $F_{\text{elc}}$ ) between a flat silica plate and a polymer thin film can be simply determined from<sup>27</sup>

$$F_{\text{elc}} = -\frac{a\sigma_s^2}{2\epsilon_0\epsilon_r} \quad (4)$$

where  $a$  is the area of contact,  $\sigma_s$  is the contact surface charge density,  $\epsilon_0$  is the permittivity of free space, and  $\epsilon_r$  is the effective dielectric constant of the contact interface, which can be obtained from<sup>27</sup>

$$\frac{D + d_p + d_{\text{si}}}{\epsilon_r} = \frac{D}{\epsilon_D} + \frac{d_p}{\epsilon_p} + \frac{d_{\text{si}}}{\epsilon_{\text{si}}} \quad (5)$$

where  $D$  is the actual separation distance between the polymer and silica, while  $d_p$  and  $d_{\text{si}}$  are the charge penetration depths in the polymer and silica, respectively. In eq 5,  $\epsilon_p$ ,  $\epsilon_{\text{si}}$ , and  $\epsilon_D$  are the dielectric constants of the polymer, silica, and separating medium, respectively. Using the simple capacitor model and further assuming the ideal conditions where no charge backflow happens upon retraction of the contacted materials from each other,<sup>12,13</sup> it was determined that the electrostatic adhesion strength (i.e., adhesion force per unit surface area) of PDMS upon contact with silica is  $4.4 \pm 0.8$  N/cm<sup>2</sup>, which is about nine times larger than that of PMMA ( $0.5 \pm 0.1$  N/cm<sup>2</sup>). With the knowledge of adhesion strength values for PDMS and PMMA and in order to estimate the magnitude of CE-generated electrostatic adhesion forces for contact of these polymers with  $7.75 \mu\text{m}$  silica particles, first we have assumed that electric charges are separated only at the contact zone between the

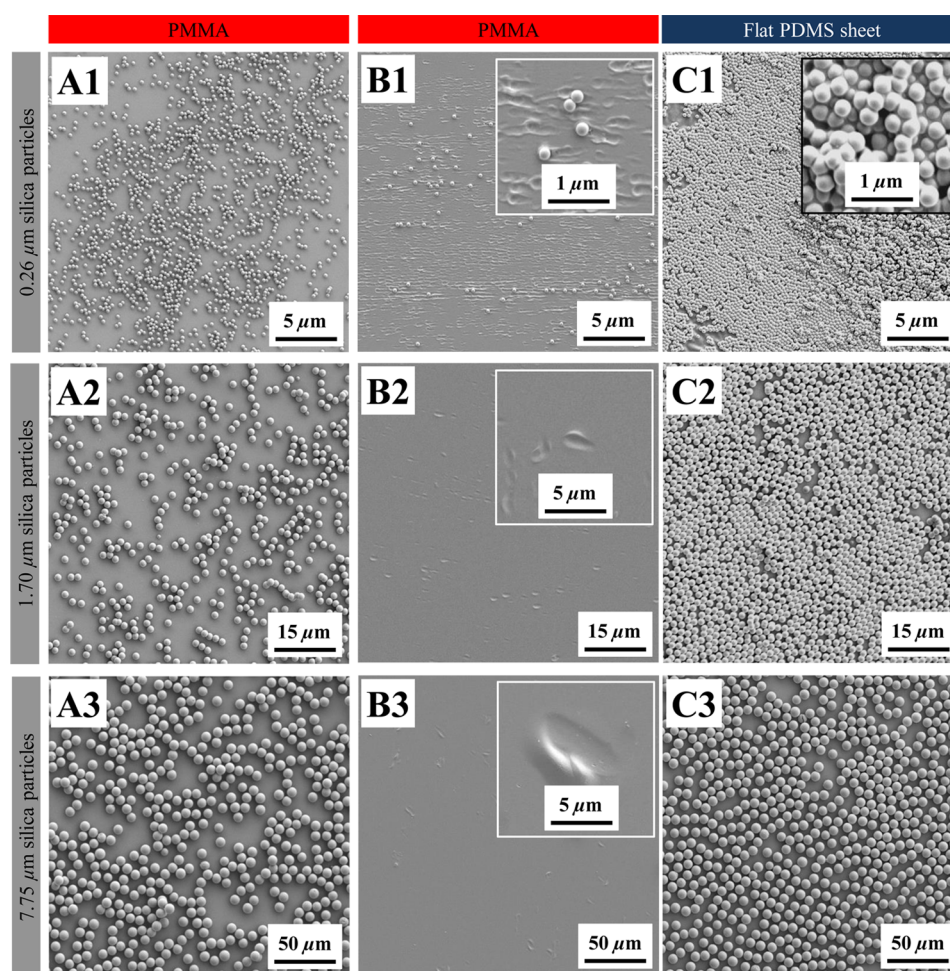


**Figure 2.** SEM images from a monolayer of (A1) 0.26, (A2) 1.70, and (A3) 7.75  $\mu\text{m}$  silica particles deposited on PMMA thin films. SEM images from the surface of PMMA thin films contaminated with silica particles, having nominal diameters of (B1) 0.26, (B2) 1.70, and (B3) 7.75  $\mu\text{m}$ , and subsequently cleaned with unstructured PDMS sheets. (C1–C3) SEM images of the surface of unstructured, flat PDMS sheets used to clean B1–B3, respectively.

particles and the polymers. Doing so, the radius of the charged area for PDMS and PMMA is considered equal to the radius of contact area for these polymers ( $\sim 1.6 \mu\text{m}$  for PDMS and  $\sim 0.2 \mu\text{m}$  for PMMA), which have been obtained using the JKR model (details can be found in the [Supporting Information](#)). By knowing the areas of contact and by approximating the contact interfaces of silica microparticles and the polymers as those between two flat parallel plates, it can be indicated that the CE-generated electrostatic forces of PDMS and PMMA upon contact with 7.75  $\mu\text{m}$  silica particles should be approximately 353.9 and 0.6 nN, respectively.

Analysis of CE-generated electrostatic interactions of PDMS and PMMA by the simple capacitor model clearly demonstrates that PDMS generates significantly larger electrostatic adhesion forces in comparison to PMMA. The relatively larger charge densities, and so the CE-driven electrostatic interaction forces of PDMS – which are still typical for an intimate contact—are most likely due to better conformability of this polymer and its propensity in formation of intimate contact with silica particles, as discussed earlier.<sup>12,13,27</sup> While the presence of surface nanostructures and the ability to develop intimate contact indirectly influence the electrostatic adhesion forces by affecting the surface charge densities, it should be noted that at the current length scales, CE-driven electrostatic forces are

independent of the separation distance and accordingly, the presence of nanoasperities at the surface (see [eq 4](#)). As a result, in this study, the effect of interfacial deformations (i.e., deformation of surface nanoasperities of PMMA and PDMS) in the estimated electrostatic adhesion strengths of these polymers has been neglected.

While the simple capacitor model has given an estimate about the CE-generated electrostatic interactions of PDMS and PMMA ( $\sim 353.9$  and 0.6 nN, respectively), finding the exact share of electrostatic forces ( $F_{\text{elc}}$ ) in the overall interfacial forces ( $F_{\text{pull-off}}$ ) of these polymers upon contact with silica microparticles is technically very challenging, if not impossible. This difficulty is mainly because of uncertainties in finding the area over which charge separation has happened. Unlike vdW forces, CE-driven electrostatic interactions are dependent on the apparent area of contact, specifically, on the area over which charge separation has happened (see [eq 4](#)). While the apparent area of contact can be simply estimated using various contact mechanics models (such as the JKR model that we employed in this study), the area of charging during contact cannot be accurately predicted for many contacts, particularly for those where the area of contact is very small, such as in our study.<sup>28,29</sup> The reason is because upon contact between two substrates, electric charges can develop outside and around the periphery

of the contact zone, as well as inside the contact zone. Although charging outside the contact zone can be practically negligible for macrocontacts, for micro/nanocontacts, this charging can be very important given that the size of the contact area and the charged area for these contacts are significantly different.<sup>28,29</sup> Despite the fact that determination of the actual area of charging during contact is not practical, a simplifying assumption can nevertheless be made in order to obtain an approximation of the magnitude of the maximum CE-driven electrostatic forces which can be generated in our system. In particular, for contact between a 7.75  $\mu\text{m}$  silica particle and PDMS or PMMA, the radius of the charged area can be considered equal to the radius of the charged particle ( $\sim 3.9 \mu\text{m}$ ). This simplifying assumption is not unrealistic, considering that for microcontacts, charging usually takes place in length scales similar to the size of the contacted objects.<sup>28,29</sup> For instance, upon contact between a  $\sim 10 \mu\text{m}$  spherical probe and a flat PMMA sample, charging over an area of  $\sim 10 \mu\text{m}$  has been reported.<sup>29</sup> Therefore, by approximating the radius of the charged area of our polymers equal to the radius of the charged particles ( $\sim 3.9 \mu\text{m}$ ), while knowing that electrostatic adhesion strengths of PDMS and PMMA are equal to  $\sim 4.4$  and  $0.5 \text{ N/cm}^2$ , respectively, it can be indicated that the maximum CE-driven electrostatic forces for PDMS and PMMA upon contact with 7.75  $\mu\text{m}$  silica particles should be approximately 2.2  $\mu\text{N}$  and 251.3 nN, respectively.

Overall, analysis of CE-driven electrostatic interactions of PDMS and PMMA indicates that the electrostatic forces of these polymers upon contact with 7.75  $\mu\text{m}$  silica particles should be in the ranges of 353.9 nN–2.2  $\mu\text{N}$  and 0.6–251.3 nN, respectively. Although finding the exact input of CE-generated electrostatic interactions in the overall interfacial interactions of these polymers is very difficult to achieve, similar to vdW forces, analysis of these forces for PDMS and PMMA clearly shows that PDMS is expected to generate significantly larger surface charge densities and accordingly electrostatic adhesion forces in comparison to PMMA. Despite the fact vdW forces of PDMS are also more effective than those of PMMA, it is highly likely that CE-driven electrostatic forces are the main interfacial forces that have allowed PDMS to develop significantly larger adhesion forces in comparison to PMMA. In fact, CE-driven electrostatic interactions are most likely the regulating interfacial interactions in the current system, given that in regular environments where dust cleaning is usually carried out, the electrostatic interactions of micrometric and submicrometric particles generally exceed the other physical interfacial forces.<sup>3</sup> However, further separate studies are required to find the exact input of vdW and electrostatic interfacial interactions in interfacial interactions of polymeric fibrillar materials and dust particles.

Given that in comparison to PMMA, PDMS generates stronger interfacial interaction forces with silica particles, regardless of the origin of these interfacial forces, it is expected that even an unstructured, flat PDMS sheet should be able to remove silica particles from the surface of a contaminated PMMA substrate. To test this hypothesis, silica microparticles of different sizes were cleaned from the surface of PMMA thin films by gently tapping unstructured PDMS sheets (used as the control samples) on various spots on the contaminated thin films. Figure 2A1–A3 show the typical scanning electron microscope (SEM) images of a monolayer of 0.26, 1.70, and 7.75  $\mu\text{m}$  silica particles deposited on PMMA thin films, while Figure 2B1–B3 show the same contaminated surfaces after they

were cleaned using unstructured PDMS sheets. As expected, the strong interfacial interactions of PDMS with silica particles allow unstructured, flat PDMS sheets to remove most of the submicrometric and almost all the micrometric contaminant particles from the PMMA substrates. Even so, the accumulation of the particles in localized regions at the surface of the PDMS sheets (see Figure 2C1–C3) result in damaging the surface of the mechanically delicate PMMA thin films, mostly in the form of small dents. It is worthwhile mentioning that the extent and density of damages formed over PMMA thin films during cleaning by flat PDMS sheets were variant between samples. These variations were expected, given that the extent and density of damages inherently depend on various factors, such as the magnitude of the applied compressive force, duration of its application, variations in the thickness of the PMMA thin films, possible solvent residue in the thin films, mechanical and material properties of the dust particles, and also the hardness of the material beneath the PMMA films. While all necessary precautions were taken to keep these variables constant in this study, the effect of the variations of these parameters on the extent and density of damages were not studied in detail as the goal of the current study is to develop a nondestructive particulate cleaning method using polymeric fibrillar materials. Therefore, we have only assessed whether there was any damage present when using flat PDMS samples to clean the substrates. Studying the extent and density of damages caused by flat PDMS sheets and investigating the factors affecting them have been left for future separate studies designed for this particular purpose.

Unlike unstructured PDMS sheets, as can be seen in Figure 3A1–A3, PDMS micropillars of controlled feature sizes (Figure 3B1–B3) do not cause any visible damage to the surface of the substrate during the cleaning process, while they effectively clean both micrometric and submicrometric contaminant particles from the surface. The nondestructive yet effective cleaning performance of PDMS micropillars is partly due to the flexible structure of these pillars. The flexibility of the fibrillar cleaning materials make possible the development of intimate contact and therefore, effective interfacial interactions of PDMS micropillars with the contaminant particles.<sup>30,31</sup> Additionally, at macroscale, fibrillar structures of current geometrical properties (i.e., flat tips with rounded edges) have been shown to generate smaller adhesion forces in comparison to flat substrates of the same material.<sup>31,32</sup> In other words, because of the particular geometrical properties of PDMS micropillars of this study, adhesion of these pillars to the substrate is smaller than that of a flat PDMS sheet to the substrate. Consequently, the adhesion-driven mechanical stresses that these micropillars may apply to the substrate upon their removal from the surface are also minimized, helping to mitigate the possibility of damage to the surface of the substrate during cleaning.

In addition to flexibility and minimal adhesion to the substrate, the other significant characteristic which allows the nondestructive cleaning by PDMS micropillars is the ability of the employed micropillars to eliminate the adsorbed particles from the tips of the pillars, and thus from the contact interface. As depicted in Figure 4A–F, when PDMS micropillars come into contact with silica particles (Figure 4B), the particles in contact with the tip of the pillars adhere to the cleaning material, due to strong interfacial interactions of PDMS with silica particles. Once the pillars are pulled away from the surface, the adhered particles become detached from the substrate (Figure 4C). However, when new particles are

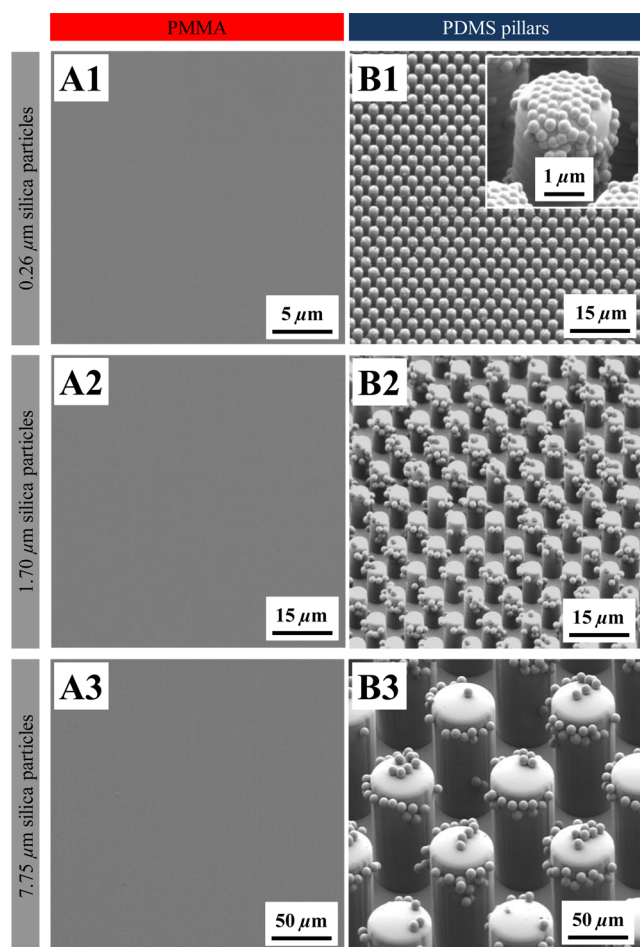


**Figure 3.** SEM images from the surface of the contaminated PMMA thin films taken after cleaning (A1) 0.26, (A2) 1.70, and (A3) 7.75  $\mu\text{m}$  silica particles from their surfaces, using PDMS pillars of (B1) 2, (B2) 5, and (B3) 50  $\mu\text{m}$  in diameter, respectively. The SEM images from the micropillars were taken from a 45° angle.

brought into contact with the pillars during the subsequent cleaning steps (Figure 4D), the previously adsorbed particles move away from the vicinity of the tip of the pillars and roll up the walls of the pillars toward the vacant area between the pillars (Figure 4E). This action prevents the accumulation of the particles at the contact interface over the course of multiple cleaning steps and accordingly, decreases the possibility of damaging the substrate during the cleaning process. It is worthwhile mentioning that the transfer of particles from the tip of the pillars to the empty space between them also makes possible the employment of small samples of a fibrillar cleaning material to clean large areas of a contaminated substrate. For instance, if the adsorbed particles are effectively moved to the vacant area between the pillars and get closely packed in that space, geometrical analysis indicates that a 1  $\text{cm}^2$  sample of 50  $\mu\text{m}$  PDMS pillars should be able to clean over 9  $\text{cm}^2$  area of a substrate contaminated with a monolayer of 7.75  $\mu\text{m}$  silica particles (see the Supporting Information for further details).

For a fibrillar cleaning material to get the adsorbed particles removed from the tip of its pillars upon multiple contacts, the fibrillar structure should have certain geometrical properties. In particular, the diameter of the cleaning pillars ( $d_{\text{pi}}$ ) should not be excessively larger than the diameter of the contaminant particles ( $d_{\text{pa}}$ ). For instance, as can be seen in Figure 5A1, a

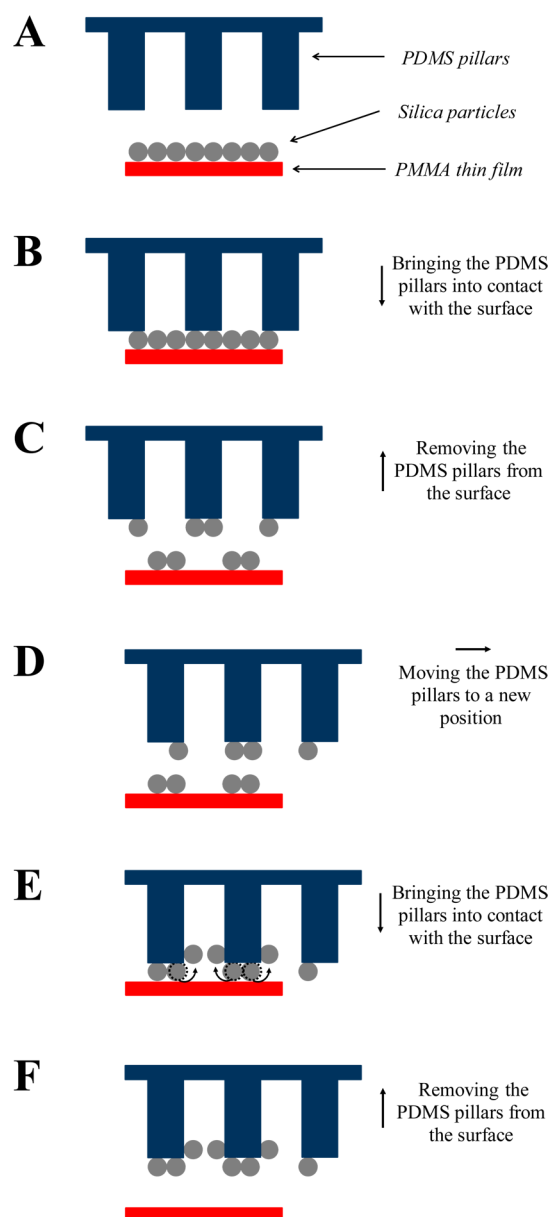


**Figure 4.** (A–F) Schematic representation of cleaning of micrometric and submicrometric silica particles from the surface of a PMMA thin film using PDMS micropillars.

PMMA substrate contaminated with 0.26  $\mu\text{m}$  particles cannot be entirely cleaned with 50  $\mu\text{m}$  PDMS pillars (further examples from other samples can be found in the Supporting Information). Since the size of the employed pillars is much larger than that of the particles ( $d_{\text{pi}}/d_{\text{pa}} \approx 192$ ), the adsorbed particles are not expelled from the tip of the pillars upon multiple contacts (see Figure 5A2). In this case, the tip of each pillar is acting as a flat substrate; limited space at the tip leads to the saturation of the tip with the relatively small particles (Figure 5A2), preventing contact between the remaining particles on the contaminated substrate and the cleaning material. Notably, the cleaning efficiency of these large micropillars in removing submicrometric particles is even lower than that of a flat substrate (compare Figure 2B1 with 5A1), because the effective contact area of the hexagonally patterned PDMS micropillars, with a wall-to-wall distance equal

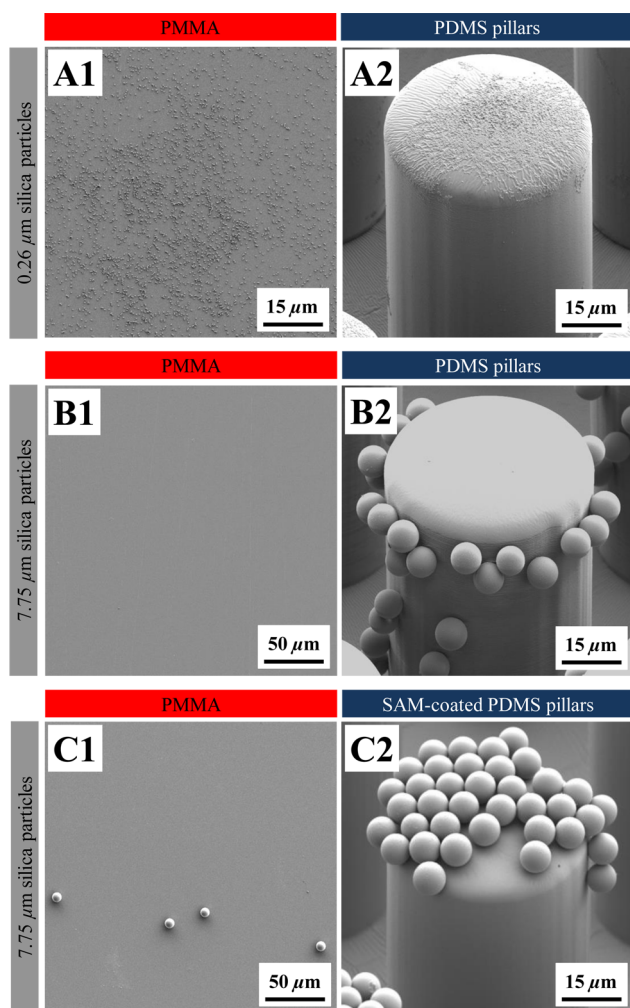


**Figure 5.** (A1) SEM image taken from the surface of a PMMA thin film, which was contaminated with 0.26  $\mu\text{m}$  silica particles and subsequently cleaned using (A2) 50  $\mu\text{m}$  PDMS pillars. (B1) Effective and nondestructive cleaning of a PMMA thin film after removing 7.75  $\mu\text{m}$  silica particles from its surface by using (B2) 50  $\mu\text{m}$  PDMS pillars. (C1) Unlike uncoated PDMS pillars, 50  $\mu\text{m}$ , FOTS-coated PDMS pillars cannot remove all 7.75  $\mu\text{m}$  silica particles from the surface of a PMMA thin film because (C2) the adsorbed particles cannot leave the vicinity of the tip of the FOTS-coated PDMS pillars. The SEM images from the micropillars were taken from a 45° angle.

to the diameter of each pillar, is  $\sim 39\%$  of that of a flat PDMS sheet.

According to our results (from systems with  $d_{\text{pi}}/d_{\text{pa}}$  values of approximately 3, 6, 8, 12, 20, and 192), it can be concluded that when the pillar diameter is less than approximately eight times larger than the particle diameter (i.e.,  $d_{\text{pi}}/d_{\text{pa}} \leq \sim 8$ ), the adsorbed particles are effectively removed from the tip of the cleaning pillars, allowing effective and nondestructive cleaning of the contaminant particles from the substrate. This is evident in Figure 5B1, which shows the successful removal of 7.75  $\mu\text{m}$  particles from the PMMA substrate by 50  $\mu\text{m}$  PDMS pillars, which were demonstrated to be ineffective in fully cleaning submicrometric particulate contaminations of 0.26  $\mu\text{m}$  from the same substrate (see Figure 5A1). As can be seen in Figure 5B2, at  $d_{\text{pi}}/d_{\text{pa}}$  of  $\sim 6$ , the relatively large, 7.75  $\mu\text{m}$  particles leave the vicinity of the tip of the pillars upon multiple contacts and as a result, the contaminant particles can be successfully transferred from the surface of the substrate to the surface of the cleaning

material, while there is no visible damage at the surface of the cleaned substrate. It is worthwhile mentioning that the transfer of microparticles from the tip to the side of micro/nanofibrils and the relation of this phenomenon to the geometrical and interfacial properties of fibrillar materials have been discussed elsewhere, mostly in studies on self-cleaning of natural and synthetic fibrillar dry adhesives.<sup>33–36</sup> However, the results of these studies have not been discussed here, given that in each of these studies, liquid and/or external mechanical loads perpendicular to the tip of the pillars were employed for the transfer and removal of the particles, while the interfacial interactions of particles and pillars were assumed to be limited to vdW interactions.<sup>33–36</sup>

Migration of particles from the tip to the wall should not only depend on the geometrical properties of the micropillars, but also on their interfacial properties. In other words, as discussed earlier, micropillars must develop strong interfacial interactions with the contaminant particles to be able to remove them from the substrate. However, if the adsorbed particles stick very strongly to the tip of the pillars, it is expected that they do not move away from the tip upon multiple contacts. As a result, effective cleaning with these pillars should not be expected. To test this hypothesis, the interfacial interactions at the surface of PDMS pillars were enhanced by improving their tendency in generating CE-driven electrostatic forces, as presumably the main source of adhesion which helps the removal of surface particulate contamination in our system. To do so, 50  $\mu\text{m}$  PDMS pillars were coated with a self-assembled monolayer (SAM) of a fluorine-based silane coupling agent (perfluorooctyltrichlorosilane, FOTS). As can be seen in Figure 5C1, the PMMA surface contaminated with 7.75  $\mu\text{m}$  silica particles can be only partially cleaned by using these comparatively stickier SAM-coated PDMS pillars. In this case, because of the strong interfacial interactions of FOTS-coated pillars with the adsorbed microparticles, the particles are not expelled from the tips of these pillars (Figure 5C2). Therefore, because of the limited effective contact area of the employed fibrillar structure ( $\sim 39\%$  of a flat surface), only partial cleaning was achieved by using these relatively stickier micropillars.

Unlike uncoated PDMS pillars, FOTS-coated PDMS pillars cannot remove the adsorbed particles from their tips because of the stronger interfacial interactions of FOTS-coated pillars in comparison to uncoated PDMS pillars. More specifically, by coating the PDMS surface with a FOTS SAM, the overall adhesion force ( $F_{\text{pull-off}}$ ) required to detach a 7.75  $\mu\text{m}$  silica particle from the cleaning material was increased to  $310.9 \pm 14.5$  nN ( $n = 10$ ) for FOTS-coated PDMS (Figure 6A), from  $270.6 \pm 10.3$  nN ( $n = 10$ ) for PDMS (Figure 1A2). The stronger adhesion of FOTS-coated PDMS pillars in comparison to uncoated PDMS pillars is not because of the changes in the vdW interaction forces caused by SAM coating, given that FOTS coating decreases the magnitude of the vdW interaction forces at the surface of PDMS. For instance, by coating the surface of PDMS with a FOTS layer, the vdW-driven jump-to-contact adhesion force ( $F_{\text{jtc}}$ )<sup>37</sup>—upon contact with a 7.75  $\mu\text{m}$  silica particle—dramatically drops from  $50.9 \pm 4.3$  nN ( $n = 10$ ) for PDMS to  $5.3 \pm 2.8$  nN ( $n = 10$ ) for FOTS-coated PDMS (see Figures 1A2 and 6A). In general, between two smooth materials of similar mechanical properties, the material with stronger vdW interactions usually generates larger jump-to-contact adhesion forces. With FOTS-coated PDMS generating smaller jump-to-contact adhesion forces in comparison to PDMS, while being even softer than PDMS (Young's modulus

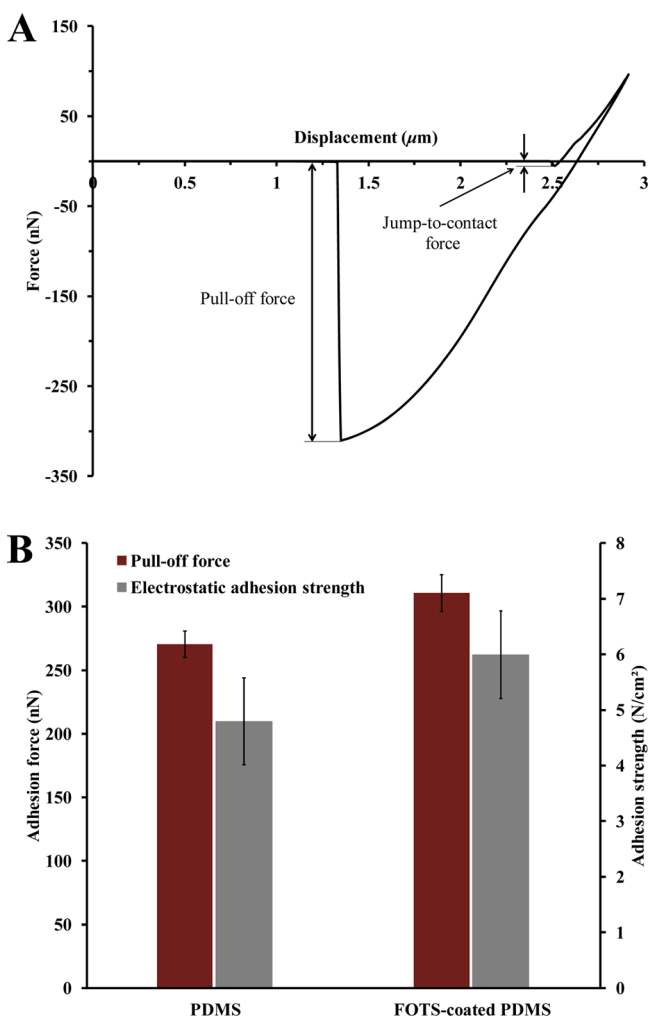


**Figure 6.** (A) Typical force vs displacement-indentation plot for a flat FOTS-coated PDMS sheet in contact with a  $7.75 \mu\text{m}$  silica particle. (B) The total pull-off force measured for contact of both PDMS and FOTS-coated PDMS with a  $7.75 \mu\text{m}$  silica particle. The electrostatic adhesion strengths for contact of uncoated and SAM-coated PDMS with silica were estimated from the charge measurement results, using the simple capacitor model.

of PDMS =  $2.7 \pm 0.3 \text{ MPa}$  ( $n = 10$ ); Young's modulus of FOTS-coated PDMS =  $0.3 \pm 0.1 \text{ MPa}$  ( $n = 10$ )), it is clear that coating the PDMS surface by FOTS has decreased the magnitude of the vdW interaction forces at the surface of PDMS.

In addition to reducing vdW interaction forces, FOTS coating also slightly decreases the propensity of the PDMS surface for forming capillary interactions, given that FOTS-coated PDMS is slightly more hydrophobic than PDMS itself ( $\theta_{\text{FOTS-PDMS}} = 111 \pm 1^\circ > \theta_{\text{PDMS}} = 108 \pm 1^\circ$  ( $n = 8$ )).<sup>10,11,21</sup>

While FOTS SAM reduces the affinity to generate both vdW and capillary interactions, like other SAMs, it can improve the surface charging, and as a result, surface electrostatic interactions.<sup>13,38,39</sup> In particular, by coating the surface of PDMS with FOTS, the CE-generated surface charge densities increased from  $1.5 \pm 0.1 \text{ mC/m}^2$  ( $n = 10$ ) for PDMS to  $1.8 \pm 0.1 \text{ mC/m}^2$  ( $n = 10$ ) for FOTS-coated PDMS. According to the simple capacitor model (eq 4) and as depicted in Figure 6B, even this slight increase in surface charging can result in significant enhancement of CE-electrostatic adhesion strengths

from  $4.4 \pm 0.8 \text{ N/cm}^2$  for PDMS to  $6.0 \pm 0.8 \text{ N/cm}^2$  for FOTS-coated PDMS, which reasonably match the experimental adhesion measurement results.

## SUMMARY

In summary, we reported a novel method for removing particulate contamination from solid surfaces using conformal, polymeric fibrillar microstructures. The strong interfacial interactions of the fabricated micropillars with the contaminant particles allow the effective removal of micrometric and submicrometric particles from the surface of the substrate. Unlike unstructured, flat sheets of the same material, polymeric micropillars do not cause any visible damage to the surface of the substrate. The cleaning performance of the fibrillar cleaning materials relies on the geometrical and interfacial properties of the fabricated micropillars, allowing the removal of the adsorbed particles away from the tip of the pillars and so the contact interface, helping to achieve nondestructive but effective cleaning.

## EXPERIMENTAL SECTION

Polydimethylsiloxane (PDMS), as two-part Sylgard 184 Silicone Elastomer Kit, was acquired from Dow Corning. Poly(methyl methacrylate) (PMMA, average molecular weight ( $M_w$ )  $\approx 350\,000$ ), anisole (ReagentPlus,  $\geq 99\%$ ), chloroform (ReagentPlus,  $\geq 99.8\%$ ), pentane (anhydrous,  $\geq 99\%$ ), trichloro(octadecyl)silane (OTS,  $\geq 90\%$ ), and trichloro(1H,1H,2H,2H-perfluorooctyl)silane (FOTS,  $\geq 97\%$ ) were purchased from Sigma. Spherical monodisperse silica microspheres, with nominal diameters of 0.26, 1.70, and  $7.75 \mu\text{m}$  (coefficient of variation  $<10\%$ ), were obtained from Cospheric LLC. Ultrasmooth, mirror-finished copper sheets (99%, 28 gauge), which had a plastic protective layer, were obtained from Fire Mountain Gems and Beads. After cutting the copper sheets into  $5 \times 5 \text{ cm}^2$  sheets and in preparation for spin-coating the polymer thin films, first the protective plastic layers were removed. Then, each sheet was cleaned individually using a commercial metal cleaner (Autosol Metal Polish from Autosol LLC).<sup>22</sup> After further cleaning by ultrasonication in pure ethanol for 40 min, the cleaned copper sheets were rinsed with ethanol and to prevent their oxidation in air, they were kept in ethanol prior to coating them with the polymers.<sup>22</sup>

For fabrication of PDMS micropillars (2, 5, 20, and  $50 \mu\text{m}$  in diameter with aspect ratios of  $\sim 2$ ), the PDMS prepolymer (with base to catalyst weight ratio of 10:1) was poured over the photolithographic silicon master-molds, containing holes of specific geometrical properties. The thickness of the polymer backing layer was adjusted to  $\sim 1.5 \text{ mm}$  by using a polytetrafluoroethylene (PTFE, Teflon) spacer. The cast polymer was degassed and then cured at  $90^\circ \text{C}$  for 120 min. Only the  $2 \mu\text{m}$  PDMS pillars were cured at  $135^\circ \text{C}$ , in order to enhance their mechanical strength and lower the chance of their collapse and buckling during the cleaning process. The polymer and the mold were cooled down to room temperature for several hours, and then the cured polymer was gently peeled off from the mold. To easily release the cured polymer from the mold, the mold was coated in advance with a self-assembled monolayer (SAM) of OTS. The mold for the fabrication of the  $2 \mu\text{m}$  PDMS pillars was coated with a SAM of FOTS instead of OTS, considering that OTS coating was not very effective for removal of these small pillars from their mold. Flat PDMS reference samples were prepared with exactly the same procedure as that used for the preparation of micropillars, but against a flat, OTS-coated silicon wafer.

In preparation for SAM-coating of the silicon molds and also flat silicon wafers with OTS, each silicon substrate was first cleaned by ultrasonication in pure chloroform at 40 kHz for 5 min, using Branson B5510 Ultrasonic Cleaner (Emerson Industrial Automation). Then, the substrate was immersed in a solution containing 0.8 mL/L of OTS in a mixture of pentane and chloroform (with 4:1 volumetric ratio). After 10 min, the sample was removed from the solution and

subsequently ultrasonicated in pure chloroform for another 10 min, in order to remove the physically adsorbed molecules from the surface. At the end, the sample was nitrogen dried and annealed under vacuum at 90 °C for 60 min. SAM-coating of the silicon mold for fabrication of the 2 μm pillars as well as that of the PDMS samples with FOTS was carried out in the gas phase, under vacuum, at 110 °C for 60 min, in the presence of 200 μL of FOTS and 500–600 μL of water. Prior to SAM-coating of the PDMS samples, they were plasma treated at high power setting for 2 min (using a PDC-32G plasma cleaner from Harrick Plasma), in order to activate the surface of the PDMS samples.

The PMMA thin films were spin-coated onto glass coverslips (2.2 × 2.2 × 0.1 cm<sup>3</sup>, from VWR International LLC.), which were plasma treated at high power setting beforehand for 1 min. PMMA solution (5 wt % PMMA in anisole) was spin-coated onto the coverslips at 1500 rpm for 30 s, using a WS-400–6NPP Spin Coater (Laurell Technologies Corporation). PMMA thin films for charge measurements, with the thickness of 4.2 ± 0.1 μm (*n* = 6), were produced from a 15 wt % solution of PMMA in anisole, which was spin-coated onto 5 × 5 cm<sup>2</sup> copper sheets at 750 rpm for 30 s. After spin-coating, all PMMA thin films were dried at 60 °C for 60 min, under a flow of nitrogen. The complete drying was achieved by heating the thin films under a flow of nitrogen for another 60 min at 160 °C, followed by 30 min annealing under vacuum at the same temperature. PDMS thin films for charge measurements, with the thickness of 5.3 ± 0.2 μm (*n* = 6), were produced by spin-coating the PDMS prepolymer (with base to catalyst weight ratio of 10:1) onto 5 × 5 cm<sup>2</sup> mirror-finished copper sheets at 7000 rpm for 30 s. PDMS thin films were then cured at 90 °C for 120 min. To prevent the oxidation of the underlying copper sheets, curing was carried out under a flow of nitrogen.

The thickness of the polymer thin films was measured by thin film step height measurement, using an Alpha-Step 200 Profilometer (KLA-Tencor Corporation).

Roughness of the polymer thin films, flat PDMS substrates, and silica substrates were estimated by atomic force microscopy (AFM) from a 5 × 5 μm<sup>2</sup> area from the surface of the samples using a Dimension FastScan Atomic Force Microscope (Bruker Corporation). The tip used for AFM imaging was a SCANASYST-AIR, silicon nitride tip (nominal tip radius = 2 nm; nominal spring constant = 0.4 N/m), obtained from Bruker Corporation. The roughness average (*R<sub>a</sub>*), maximum peak height (*R<sub>p</sub>*), and root-mean-square roughness parameter (*R<sub>RMS</sub>*) for each sample was estimated by analyzing the obtained AFM images using Nanoscope Analysis, version 1.5 (Bruker Corporation). After applying third-order *Flatten* and *Plane Fit* functions to each image, the built-in *Roughness*, *Power Spectral Density (PSD)*, and *Peak* commands were employed to determine the corresponding *R<sub>a</sub>*, *R<sub>p</sub>*, and *R<sub>RMS</sub>* values, respectively.

Polarity characteristics (i.e., hydrophobicity and hydrophilicity) of the PMMA thin films as well as those of the cleaning materials and silica substrates were determined by water contact angle measurement tests, consisting the measurement of the static contact angle of a (6–10 μL) water droplet by a NRL Contact Angle Goniometer (Ramé-Hart, Inc.).

Contamination of PMMA thin films with silica particles was achieved by first soiling an aluminum foil with the silica particles of the choice. After shaking the aluminum foil to attain an almost a monolayer of particles on the foil, the PMMA thin film (which was electrostatically charged beforehand with a soft nylon brush (6150 FAN from Princeton Artist Brush Company)) was gently brought into contact with the particles on the aluminum foil, and then slowly removed. The static charges at the surface of the particles as well as those at the surface of the PMMA thin films were subsequently discharged using a Zerostat 3 Antistatic Gun (Armour Home Electronics, Ltd.). For the sake of simplicity, in this study, only spherical silica microparticles of controlled geometrical properties were employed as the contaminant particles. However, one should bear in mind that natural dust particles usually have more complicated chemical, physical, and geometrical properties.

To clean silica particles from the contaminated PMMA thin films with either flat PDMS sheets or PDMS micropillars, first a stripe of the cleaning material (6 cm in length and 2 cm in width) was folded onto

its back to make a droplet shape. Then, the folded stripe was gently tapped 50 times on various spots on the surface of the contaminated thin film in order to remove the deposited silica particles from the surface. Considering that cleaning quality should be dependent on the time between the surface soiling and cleaning, all cleaning experiments in this study were performed within 1–2 min after the contamination of the substrates with silica particles. All cleaning experiments were independently replicated at least three times. The cleaning quality was investigated by scanning electron microscope (SEM) imaging from the surface of both the substrate and the cleaning material, performed on an Ultra-High-Resolution Analytical FE-SEM (SU-70, Hitachi High-Technologies Corporation) operating at 2 kV. In preparation for SEM imaging, each sample was coated with a thin (~20 nm) chromium layer, which was sputtered on the sample by a Desk V sputtering instrument from Denton Vacuum, LLC.

For AFM adhesion force measurements, tipless silicon nitride cantilevers (NP-O from Bruker Corporation) were first cleaned in an UV/ozone cleaner (BioForce Nanosciences) for 20 min. Then, a 7.75 μm silica particle was glued to the tip of the “A” cantilever (nominal frequency = 65 kHz; nominal spring constant = 0.35 N/m), using UV-curable adhesive (Norland Optical Adhesive 68 from Norland Products Inc.), and cured for 20 min in the UV/ozone cleaner. All particle-functionalized AFM cantilevers were prepared according to a procedure previously described.<sup>40</sup> Adhesion forces between the samples and the silica-functionalized cantilevers were measured on a Dimension Icon AFM instrument (Bruker Corporation). Before adhesion test measurements, the possible static charges at the surface of the particle as well as those at the surface of the substrate were discharged using a Zerostat 3 Antistatic Gun (Armour Home Electronics Ltd.). The cantilever deflection sensitivity and spring constant were determined for each cantilever using the thermal noise method.<sup>41</sup> Force measurements were collected using a trigger force of 100 nN, a ramp size of 5 μm, and a ramp rate of 0.5 Hz. Adhesion force traces (see Figures 1A1 and 1A2 and Figure 6A) were determined by converting curves of cantilever deflection vs piezoelectric stage retraction to force vs displacement, using Nanoscope Analysis Version 1.5 (Bruker Corporation). Zero-displacement points in adhesion force plots were set at ~2.5 μm before the jump-to-contact phenomenon happens. The zero-displacement of approximately 2.5 μm was chosen only for visual clarity, so the results for different samples can be visually compared with each other. The Young's modulus of the unstructured, flat PDMS samples (2.7 ± 0.3 MPa (*n* = 10)) and that of the flat FOTS-coated PDMS samples (0.3 ± 0.1 MPa (*n* = 10)) were estimated using Nanoscope Analysis Version 1.5, by fitting the Hertzian model<sup>42</sup> in the force vs displacement indentation plots, considering the material Poisson's ratio of 0.5.<sup>43</sup>

Charge measurements for PDMS, PMMA, and FOTS-coated PDMS were performed by gently placing an optical-grade, polished silica disc (25.4 mm in diameter, 3.2 mm in thickness, from Ted Pella, Inc.) on the corresponding polymer thin films which were coated on ultrapolished copper sheets. Once a silica disc was brought into contact with a polymer thin film, electric charges were separated at the contact interface and subsequently penetrated up to a certain depth into the polymer thin film and the contacted silica disc, which results in induction of an image charge on the copper sheet under the polymer thin film. While the silica disc and the polymer thin film were still in contact, the density of the image charges that were induced in the backing copper sheet ( $\sigma_{\text{image}}$ ) were recorded by a 6517B Electrometer/High Resistance Meter (Keithley Instruments), connected to the back of the copper sheet. Using the measured  $\sigma_{\text{image}}$  and neglecting the effect of charge backflow via tunneling,<sup>23,44</sup> the actual surface charge density over the polymer ( $\sigma_s$ ) during contact was determined by<sup>45</sup>

$$\sigma_s = \frac{\sigma_{\text{image}}}{\left( \frac{D + d_p + d_{\text{si}}}{\left( \frac{h_p - d_p}{\epsilon_p} - \frac{d_{\text{si}}}{\epsilon_{\text{si}}} + \frac{D}{\epsilon_{\text{D}}} \right)} \right)} \quad (6)$$

where  $D$  is the actual separation distance between the silica disc and the thin film;  $d_p$  and  $d_{si}$  are the charge penetration depths in the polymer thin film and silica, respectively. In eq 6,  $h_p$  is the thickness of the polymer thin film, while  $\epsilon_p$ ,  $\epsilon_{si}$ , and  $\epsilon_D$  are the dielectric constants of the polymer, the silica disc, and the separating medium, respectively. Further details about charge backflow can be found in the literature.<sup>25</sup> In calculating the surface charge densities using eq 6, since both the silica and polymer surfaces were smooth, the actual separation distance ( $D$ ) was considered as that of the interatomic separation distance of  $\sim 0.3$  nm.<sup>10</sup> The charge penetration depths,  $d_p$  and  $d_{si}$ , were considered equal and approximated by 3 nm,<sup>46</sup> while the dielectric constant of the separating medium ( $\epsilon_D$ ) was considered equal to 1, the dielectric constant of air. It should be noted that at the relative humidity (RH) of  $10 \pm 1\%$  where the experiments were carried out, it is expected that small amounts of water get adsorbed over the polymer thin films and silica discs.<sup>11,21</sup> However, since at this low humidity level, the thickness of the adsorbed layer of water is typically less than 0.2 nm (roughly a thickness of a monolayer of water)<sup>21</sup> and seeing that the dielectric constant of a monolayer of water ( $\sim 6$ ) is not very high (as that of the bulk of water ( $\sim 80$ )), the presence of water at the interface was ignored, given that the effect of its incorporation in charge measurements was negligible.<sup>27</sup> Before performing charge measurement tests, both the polymer thin films and silica substrates were discharged (using a Zerostat 3 Antistatic Gun (Armour Home Electronics Ltd.)) to remove any static charge which may have built up on them.

Similar to charge measurements, in calculations of contact electrification-driven adhesion forces (eq 4 and 5), the dielectric constant of the separating medium ( $\epsilon_D$ ) was considered similar to the dielectric constant of air (which is equal to 1). However, if it is considered that a water monolayer is present at the contact interface, the dielectric constant of the separating medium ( $\epsilon_D$ ) would be a little larger and so, the calculated adhesion strength values, which were determined using eq 4, would be slightly smaller, although they still completely supports our conclusions. In particular, when having a monolayer of water at the contact interface, the effective dielectric constant ( $\epsilon_e$ ) for PDMS/silica and PMMA/silica would increase to only 3.2 (from 2.9) and 4.0 (from 3.4), respectively, leading to very negligible decline in the calculated adhesion strength values for both PDMS and PMMA.

## ■ ASSOCIATED CONTENT

### ● Supporting Information

The Supporting Information is available free of charge on the ACS Publications website at DOI: 10.1021/acsami.5b09154.

Estimation of the adhesive and geometrical properties of PDMS/silica and PMMA/silica interfaces using the JKR model, calculations of the area of a contaminated surface that can be cleaned using a unit surface area of a polymeric sheet patterned with pillars, AFM images from contaminated PMMA thin films taken before and after cleaning, as well as additional SEM images from the contaminated substrates and the cleaning materials taken after cleaning (PDF)

## ■ AUTHOR INFORMATION

### Corresponding Author

\*E-mail: kyle.vanderlick@yale.edu.

### Author Contributions

The manuscript was written through contributions of all authors. All authors have given approval to the final version of the manuscript.

### Notes

The authors declare no competing financial interest.

## ■ ACKNOWLEDGMENTS

The authors thank Dr. Anikó Bezur and Dr. Paul Whitmore for their thoughtful discussions.

## ■ REFERENCES

- (1) Mittal, K. L. *Treatise on Clean Surface Technology*; Plenum Press: USA, 1987.
- (2) Mittal, K. L. *Particles on Surfaces: Detection, Adhesion, and Removal*; Plenum Press: USA, 1994.
- (3) Kohli, R.; Mittal, K. L. *Developments in Surface Contamination and Cleaning: Fundamentals and Applied Aspects*; William Andrew: USA, 2008.
- (4) Kohli, R.; Mittal, K. L. *Developments in Surface Contamination and Cleaning: Methods for Removal of Particle Contaminants*; William Andrew: UK, 2011.
- (5) Pulker, H. K. *Coatings on Glass*; Elsevier: Netherlands, 1999.
- (6) Gale, G. W.; Busnaina, A. A. Removal of Particulate Contaminants using Ultrasonics and Megasonics: A Review. *Part. Sci. Technol.* **1995**, *13*, 197–211.
- (7) Tam, A. C.; Leung, W. P.; Zapka, W.; Ziemlich, W. Laser-Cleaning Techniques for Removal of Surface Particulates. *J. Appl. Phys.* **1992**, *71*, 3515–3523.
- (8) Sherman, R.; Grob, J.; Whitlock, W. Dry Surface Cleaning using CO<sub>2</sub> Snow. *J. Vac. Sci. Technol., B: Microelectron. Process. Phenom.* **1991**, *9*, 1970–1977.
- (9) Mosbacher, M.; Münzer, H.; Zimmermann, J.; Solis, J.; Boneberg, J.; Leiderer, P. Optical Field Enhancement Effects in Laser-Assisted Particle Removal. *Appl. Phys. A: Mater. Sci. Process.* **2001**, *72*, 41–44.
- (10) Israelachvili, J. N. *Intermolecular and Surface Forces*; Academic Press: USA, 2011.
- (11) Zimon, A. D. *Adhesion of Dust and Powder*; Plenum: USA, 1982.
- (12) Horn, R. G.; Smith, D. T. Contact Electrification and Adhesion between Dissimilar Materials. *Science* **1992**, *256*, 362–364.
- (13) Horn, R. G.; Smith, D. T.; Grabbe, A. Contact Electrification Induced by Monolayer Modification of a Surface and Relation to Acid-Base Interactions. *Nature* **1993**, *366*, 442–443.
- (14) From the Product Specifications Reported by the Producer.
- (15) Clayton, L. M.; Sikder, A. K.; Kumar, A.; Cinke, M.; Meyyappan, M.; Gerasimov, T. G.; Harmon, J. P. Transparent Poly (Methyl Methacrylate)/Single-Walled Carbon Nanotube (PMMA/SWNT) Composite Films with Increased Dielectric Constants. *Adv. Funct. Mater.* **2005**, *15*, 101–106.
- (16) Johnson, K.; Kendall, K.; Roberts, A. Surface Energy and the Contact of Elastic Solids. *Proc. R. Soc. London, Ser. A* **1971**, *324*, 301–313.
- (17) Zappone, B.; Rosenberg, K. J.; Israelachvili, J. Role of Nanometer Roughness on the Adhesion and Friction of a Rough Polymer Surface and a Molecularly Smooth Mica Surface. *Tribol. Lett.* **2007**, *26*, 191–201.
- (18) Rabinovich, Y. I.; Adler, J. J.; Ata, A.; Singh, R. K.; Moudgil, B. M. Adhesion between Nanoscale Rough Surfaces: I. Role of Asperity Geometry. *J. Colloid Interface Sci.* **2000**, *232*, 10–16.
- (19) Haynes, W. M. *CRC Handbook of Chemistry and Physics*; CRC Press: USA, 2014.
- (20) Drelich, J. Adhesion Forces Measured between Particles and Substrates with Nano-Roughness. *Miner. Metall. Process.* **2006**, *23*, 226–232.
- (21) Huber, G.; Mantz, H.; Spolenak, R.; Mecke, K.; Jacobs, K.; Gorb, S. N.; Arzt, E. Evidence for Capillarity Contributions to Gecko Adhesion from Single Spatula Nanomechanical Measurements. *Proc. Natl. Acad. Sci. U. S. A.* **2005**, *102*, 16293–16296.
- (22) Apodaca, M. M.; Wesson, P. J.; Bishop, K. J.; Ratner, M. A.; Grzybowski, B. A. Contact Electrification between Identical Materials. *Angew. Chem.* **2010**, *122*, 958–961.
- (23) Lowell, J.; Rose-Innes, A. Contact Electrification. *Adv. Phys.* **1980**, *29*, 947–1023.

- (24) Izadi, H.; Golmakani, M.; Penlidis, A. Enhanced Adhesion and Friction by Electrostatic Interactions of Double-Level Teflon Nanopillars. *Soft Matter* **2013**, *9*, 1985–1996.
- (25) Izadi, H.; Penlidis, A. Polymeric Bio-Inspired Dry Adhesives: Van der Waals or Electrostatic Interactions? *Macromol. React. Eng.* **2013**, *7*, 588–608.
- (26) Lacks, D. J.; Mohan Sankaran, R. M. Contact Electrification of Insulating Materials. *J. Phys. D: Appl. Phys.* **2011**, *44*, 453001.
- (27) Izadi, H.; Stewart, K. M.; Penlidis, A. Role of Contact Electrification and Electrostatic Interactions in Gecko Adhesion. *J. R. Soc., Interface* **2014**, *11*, 20140371.
- (28) Schönenberger, C. Charge Flow during Metal-Insulator Contact. *Phys. Rev. B: Condens. Matter Mater. Phys.* **1992**, *45*, 3861.
- (29) Terris, B.; Stern, J.; Rugar, D.; Mamin, H. Contact Electrification using Force Microscopy. *Phys. Rev. Lett.* **1989**, *63*, 2669.
- (30) Hu, S.; Xia, Z. Rational Design and Nanofabrication of Gecko-Inspired Fibrillar Adhesives. *Small* **2012**, *8*, 2464–2468.
- (31) Boesel, L. F.; Greiner, C.; Arzt, E.; del Campo, A. Gecko-Inspired Surfaces: A Path to Strong and Reversible Dry Adhesives. *Adv. Mater.* **2010**, *22*, 2125–2137.
- (32) del Campo, A.; Greiner, C.; Arzt, E. Contact Shape Controls Adhesion of Bioinspired Fibrillar Surfaces. *Langmuir* **2007**, *23*, 10235–10243.
- (33) Hansen, W.; Autumn, K. Evidence for Self-Cleaning in Gecko Setae. *Proc. Natl. Acad. Sci. U. S. A.* **2005**, *102*, 385–389.
- (34) Hu, S.; Lopez, S.; Niewiarowski, P. H.; Xia, Z. Dynamic Self-Cleaning in Gecko Setae via Digital Hyperextension. *J. R. Soc., Interface* **2012**, *9*, 2781–2790.
- (35) Menguc, Y.; Rohrig, M.; Abusomwan, U.; Holscher, H.; Sitti, M. Staying Sticky: Contact Self-Cleaning of Gecko-Inspired Adhesives. *J. R. Soc., Interface* **2014**, *11*, 20131205.
- (36) Abusomwan, U. A.; Sitti, M. Mechanics of Load-Drag-Unload Contact Cleaning of Gecko-Inspired Fibrillar Adhesives. *Langmuir* **2014**, *30*, 11913–11918.
- (37) Landman, U.; Luedtke, W. D.; Burnham, N. A.; Colton, R. J. Atomistic Mechanisms and Dynamics of Adhesion, Nanoindentation, and Fracture. *Science* **1990**, *248*, 454–461.
- (38) Thomas, S. W.; Vella, S. J.; Kaufman, G. K.; Whitesides, G. M. Patterns of Electrostatic Charge and Discharge in Contact Electrification. *Angew. Chem.* **2008**, *120*, 6756–6758.
- (39) Thomas, S. W., III; Vella, S. J.; Dickey, M. D.; Kaufman, G. K.; Whitesides, G. M. Controlling the Kinetics of Contact Electrification with Patterned Surfaces. *J. Am. Chem. Soc.* **2009**, *131*, 8746–8747.
- (40) Li, Q.; Elimelech, M. Organic Fouling and Chemical Cleaning of Nanofiltration Membranes: Measurements and Mechanisms. *Environ. Sci. Technol.* **2004**, *38*, 4683–4693.
- (41) Hutter, J. L.; Bechhoefer, J. Calibration of Atomic-Force Microscope Tips. *Rev. Sci. Instrum.* **1993**, *64*, 1868–1873.
- (42) Hertz, H. *Miscellaneous Papers*; Macmillan: UK, 1896.
- (43) Greiner, C.; del Campo, A.; Arzt, E. Adhesion of Bioinspired Micropatterned Surfaces: Effects of Pillar Radius, Aspect Ratio, and Preload. *Langmuir* **2007**, *23*, 3495–3502.
- (44) Baytekin, H. T.; Baytekin, B.; Soh, S.; Grzybowski, B. A. Is Water Necessary for Contact Electrification? *Angew. Chem., Int. Ed.* **2011**, *50*, 6766–6770.
- (45) Ireland, P. M. Contact Charge Accumulation and Separation Discharge. *J. Electrostat.* **2009**, *67*, 462–467.
- (46) Brennan, W.; Lowell, J.; O'Neill, M.; Wilson, M. Contact Electrification: The Charge Penetration Depth. *J. Phys. D: Appl. Phys.* **1992**, *25*, 1513.